Computational study of iminium ion formation: effects of amine structure

Gareth J. S. Evans, Katherine White, James A. Platts* and Nicholas C. O. Tomkinson

Received 21st February 2006, Accepted 10th May 2006
First published as an Advance Article on the web 1st June 2006
DOI: 10.1039/b602645a

Density functional calculations are used to explore the formation of iminium ions from secondary amines and acrolein and the subsequent reactivity of the resulting iminium ions. After establishing a feasible profile for this reaction in simulated experimental conditions, we focus on the effect of variation in amine structure on calculated barriers. This analysis shows that incorporation of a heteroatom (N or O) in the α-position to the reactive amine results in significantly reduced energy barriers, as does an electron-withdrawing group (carbonyl or thiocarbonyl) in the β-position. Electron density analysis is used to monitor reactions at a detailed level, and to identify important intermolecular interactions at both minima and transition states. Barriers to reaction are linked to calculated proton affinities of secondary amines, suggesting that the relative ease of protonation–deprotonation of the amine is a key property of effective catalysts. Moreover, barriers for subsequent Diels–Alder reaction of iminium ions with cyclopentadiene are lower than for their formation, suggesting that formation may be the rate determining step in the catalytic cycle.

Introduction

Much interest has been shown in metal-free asymmetric catalysis in recent times.[1] Organic transformations through the use of small organic molecules has proven to be an exciting and fast paced field.[2,3] Organocataylsis has been used in numerous reactions[4–10] to give the products in excellent yield and enantiometric excess. Many of the reactions that have been developed were previously only accessible through metal-based reactions or in some cases not feasible through the use of Lewis acid catalysis.[11] As progress is made in the development of the portfolio of reactions available, and the range of possible substrates for these reactions is widened, effort can be turned to increasing reaction rates and at the same time decreasing catalyst loading.

Our group has undertaken research into this area from both synthetic and theoretical directions. Recent work has focused on the use of iminium ions: catalysis using these ions exploits the higher reactivity of iminium ions compared to their parent carbonyl species, facilitating cycloaddition and nucleophilic addition reactions.[1] Synthetic studies have shown highly promising rates and yields using this approach. Iminium ions are formed *via* the reaction of amines and carbonyl compounds (see Scheme 1). We have recently shown that a heteroatom such as *N* or *O* at the α-position to the reactive amine centre has a marked effect on catalytic activity.[12] This can be further enhanced by the presence of an electron-withdrawing group such as a carbonyl in the β-position, giving rise to increased selectivity and reaction rates whilst allowing for a decrease in catalyst loading.[12] Quantifying effects of amine structure and functional groups upon the formation of the reactive species has been a goal in our research.

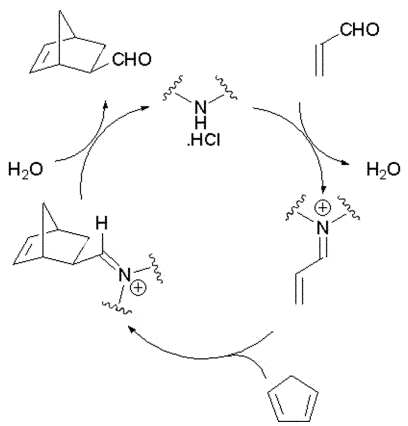

Scheme 1 General reaction scheme of iminium ion catalysed Diels–Alder reaction.

In this work, we employ standard conditions of low pH, with the amine present as a salt, usually of hydrochloric acid, though other acids have been used. Jencks[13] gives an outline mechanism for formation of 'imines' from carbonyls and strong amine bases in acidic conditions, in which attack of the amine at the carbonyl is rate-determining, followed by or concerted with proton transfer to form a tetrahedral intermediate containing a C–N single bond. Loss of water to form the iminium ion is then rapid in acidic aqueous solution. To date, most theoretical studies of iminium ions have concentrated on their reactivity in *e.g.* aldol and Diels–Alder reactions,[14,15] with less emphasis on the formation of the iminium ion itself. This is somewhat surprising as this step has been proposed as the rate-determining step within the catalytic cycle (Scheme 1).[5] Boyd and co-workers[16] have calculated such a pathway, but used basic conditions in which the amine is present as the free base.

In this work, density functional calculations were performed to determine a possible mechanism for acid-catalysed iminium

School of Chemistry, Cardiff University, Park Place, Cardiff, CF10 3AT, UK. E-mail: platts@cardiff.ac.uk; Fax: +44-2920-874030; Tel: +44-2920-874950

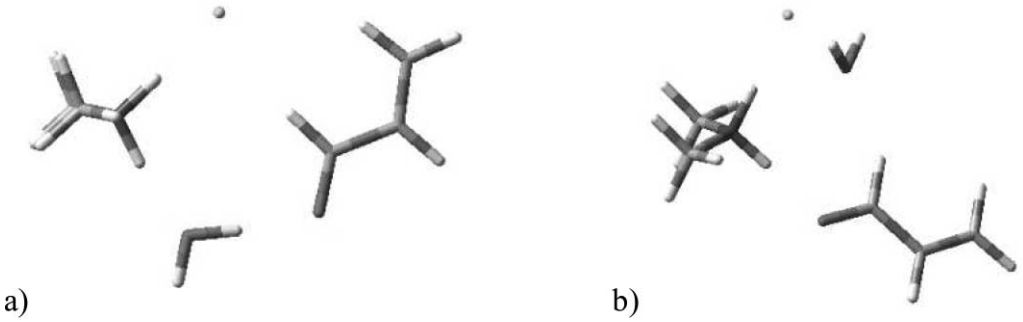

Fig. 1 Two optimised reactant geometries differing in energy by 2.9 kJ mol^{-1}.

ion formation from carbonyls and amine-hydrochloride salts, and hence to understand and predict how amine structure might influence the energetics and kinetics of iminium ion formation. Following this, a second goal was to develop a predictive scale of amine reactivity based upon structure, functionality, and calculated properties. In the process of carrying out these calculations, a number of theory levels, basis sets and solvent models were tested. Preliminary calculations on subsequent Diels–Alder reaction of iminium ions are also presented.

Computational methods

All calculations used density functional theory (DFT) methods and were carried out using the Gaussian03 package.[17] Initial optimisations and transition state searches were carried out at the B3LYP/6-31+G(d,p) level,[18–20] within an Onsager solvent shell of methanol.[21] Subsequent calculations used to test these methods employed the larger 6-311++G(2d,p) basis set,[20] as well as the mPW1PW91 functional[22] and an alternative PCM model of methanol solvation.[23] Transition states connecting minima were located using a quadratic synchronous transit (QST3) approach,[24,25] specifying reactant and product structures along with a guess of a transition state obtained from relaxed potential energy surface (PES) scans. In order to check whether a transition state (TS) located did indeed link the expected reactants and products, the TS geometry was perturbed both forwards and backwards along the transition vector, then a geometry optimisation was performed on the resulting co-ordinates.

AIM2000[26] was used to perform atoms in molecules (AIM) analysis, as developed by Bader *et al.*,[27,28] in order to evaluate inter- and intramolecular interactions in the system. Using this method, underlying reasons for observed energetic and geometric differences could be identified and phenomena such as intermolecular hydrogen bonding interactions could be examined. AIM theory is based on the partitioning of electron density (ρ) into well-defined regions, bounded by surfaces of zero-flux in the electron density. Analysis of ρ and its gradient reveals features such as minima, maxima and saddle points, known as critical points (CPs). Of particular interest are bond critical points (BCPs), which define the interaction of two nuclear attractors, and can give information on bond strength and order.[28,29] Throughout this work, we have made use of the observation that increased ρ at a BCP indicates an increase in bond order, as shown by Bader[30] and Cremer and Kraka.[31] An example of such relationships can be seen for many diverse types of bond.[29]

Results and discussion

We started our theoretical investigations with a realistic model of the reaction conditions used in the acid-catalysed formation of iminium ions in wet methanol. An ensemble was constructed containing the hydrochloride salt of the simplest secondary amine; dimethylamine, acrolein as a model electrophile, and a single explicit water molecule. These reactants in the model system can be rearranged in many ways, the most mobile aspects of the ensemble being the chloride ion and water molecule, meaning that throughout the initial calculations all low energy geometries had the reacting species (amine plus acrolein) in approximately the same orientation. Optimisation of this reaction mixture from varying starting points revealed many stable conformations within 5 kJmol^{-1} of each other, and with negligible barriers of interconversion (see Fig. 1).

Although the lowest energy geometry was a stable minimum, the positioning of the chloride ion meant that further reaction gave substantially higher barriers than found for the next lowest energy geometry, the difference in energy between these two minima being 2.9 kJ mol^{-1}. On minimisation the reactants form a hydrogen bonded complex. Non-bonding interactions play an important role in the stabilisation and orientation of reactants at stationary points: the chloride ion positions over one proton of the protonated amine, the carbonyl oxygen of acrolein aligns with the remaining N–H, and the main body of acrolein stretches away from the amine with the α-hydrogen coordinating with the water molecule (Fig. 1b).

In order to determine whether a single explicit water molecule was sufficient to model the behaviour of wet methanol, the effect of additional water molecules on the mixture was evaluated by adding a further three waters to the system. In all cases, optimisation led to the chloride occupying a comparable position as the simple system, *i.e.* forming a close contact with the protonated amine (Cl$\cdots$H distances vary between 2.17 Å and 1.90 Å), with minor changes in other geometrical details (Fig. 2). Another possibility for a model system was to exclude the explicit water in favour of a simpler system. Calculations of this system were carried out giving very similar barriers to the later stages of the pathway. Although such a system has less complexity, the same number of minima was found as in the hydrated system. It was therefore decided to continue with the explicit water as this contained the species present in the experimental reaction mixture.

Using the reactant ensemble shown in Fig. 1b, a pathway containing seven stationary points was determined. Local minima

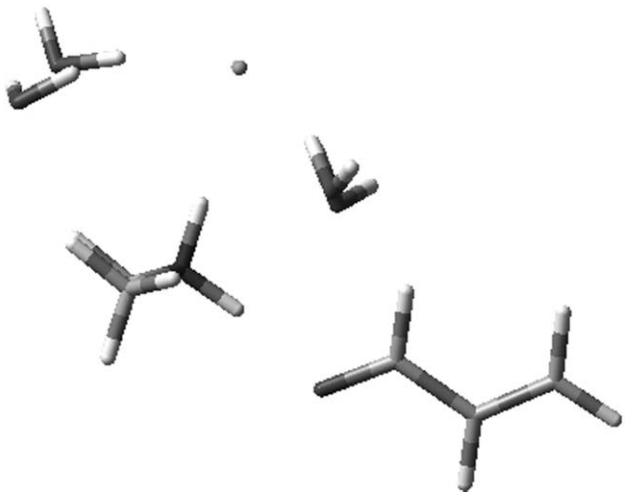

Fig. 2 Geometry of reactants plus four water molecules.

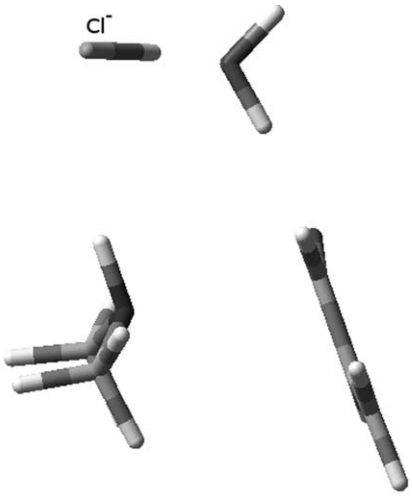

Fig. 4 Intermediate geometry.

corresponding to the iminium ion product, and an intermediate structure containing a C–N single bond (which we term 'aminol'), as well as the reactant geometry shown above, were located and confirmed *via* harmonic frequency calculation. Using the QST procedure, a transition state (TS1, shown in Fig. 3) linking the reactant and aminol intermediate was located, with a single imaginary frequency of 139.9i cm^{-1}. TS1 is 110 kJ mol^{-1} higher in energy than the reactant complex, a sizeable barrier due to the transfer of a proton from the amine to chloride, accompanied by a small re-orientation of acrolein and water. The chloride is covalently bound to the hydrogen with an H–Cl distance of 1.318 Å (*cf.* 1.288 Å for free HCl at the same level). The process of the chloride removing one of the protons forces the amine to 'rock back' to accommodate this change. Hydrogen bonding between the transferring proton and the carbonyl oxygen ($H \cdots O = 1.957$ Å) and between the proton and the free nitrogen of the amine ($H \cdots N = 1.659$ Å) can be observed.

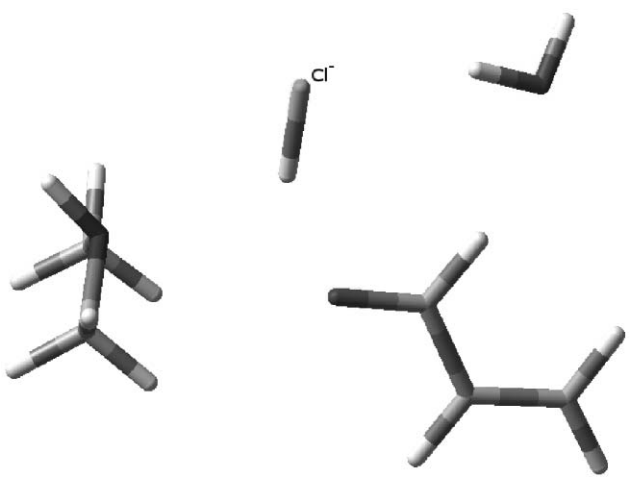

Fig. 3 Geometry of TS1.

Perturbing TS1 in the forward direction led not to the expected aminol structure, but instead to an unexpected local minimum, as shown in Fig. 4. This structure has an energy 32.6 kJ mol^{-1} below TS1, has no imaginary vibrational frequencies, and differs from that of TS1 solely by rotation of the various moieties, with both acrolein and HCl rotated towards their subsequent orientations. As the amine is symmetric, the two possible directions in which the acrolein may rotate are degenerate, though this will become an important point for unsymmetrical amines. This intermediate shows a reordering of weak interactions from TS1, including N–$H \cdots Cl$ (2.702 Å). At this stage the water molecule performs a role by bridging the hydrogen chloride (Cl–$H \cdots O = 1.591$ Å) and the carbonyl (O–$H \cdots O = 1.703$ Å).

TS2 (Fig. 5) separates this metastable intermediate structure from the aminol species: the barrier from intermediate to TS2 was just 10 kJ mol^{-1}, *i.e.* essentially negligible when compared to the barrier associated with TS1. The structure of this transition state was of interest, the water molecule mediates proton transfer from HCl to the carbonyl oxygen, acting as a "proton shuttle". Thus,

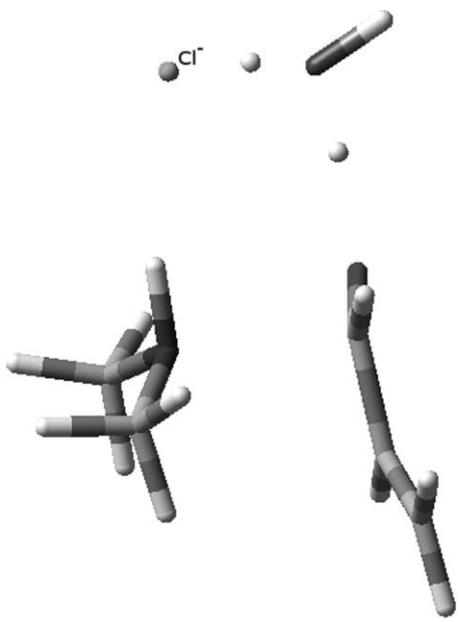

Fig. 5 TS2 geometry.

it appears that only this step requires the presence of an explicit water molecule, and hence explains the action of trace water in the reaction mixture noted previously.[12] A single imaginary frequency is found as 312.9i cm^{-1}.

The aminol structure is *ca.* 10 kJ mol^{-1} higher in energy than the reactant complex: the N–C bond has formed in this species and a proton transferred from amine to carbonyl (Fig. 6). Here again, the chloride ion is closely associated with the protonated amine centre, with the water hydrogen bonded to both Cl^- and OH. The N–C bond length is 1.56 Å, *i.e.* somewhat longer than a typical N–C single bond (1.46 Å in methylamine, calculated at the same theoretical level). The reactive carbon centre has an approximate sp^3 geometry (NCO = 109.0°, NCC = 111.4°). Perturbation along the reaction coordinate forward from TS2 results in the aminol geometry shown in Fig. 6, but two other conformations can be located. Of these three conformations, the two with H–N–C–O torsion angles of +71.4° and −64.9° are of essentially equal energy, while that with −171.6° is considerably higher in energy. Barriers of 40 kJ mol^{-1} and 54 kJ mol^{-1} separate these minima, such that effective free rotation around the C–N bond is anticipated.

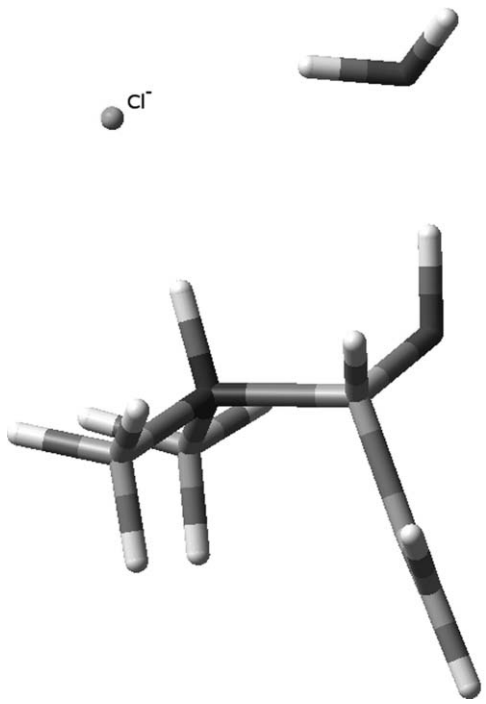

Fig. 6 Aminol geometry.

The final transition state located, TS3 (Fig. 7), accompanies elimination of water from the aminol intermediate. This is again a proton transfer from amine to oxygen (Cl···H = 1.527 Å, O···H = 1.248 Å), mediated by the presence of chloride. TS3 is *ca.* 90 kJ mol^{-1} above the aminol species. Thus, the barrier associated with initial formation of the N–C bond is rather higher in energy than subsequent elimination of water to the final product. The N–C distance reduces to 1.390 Å and the carbon chain of the acrolein begins to flatten. A single imaginary frequency of 405.62i cm^{-1} is found.

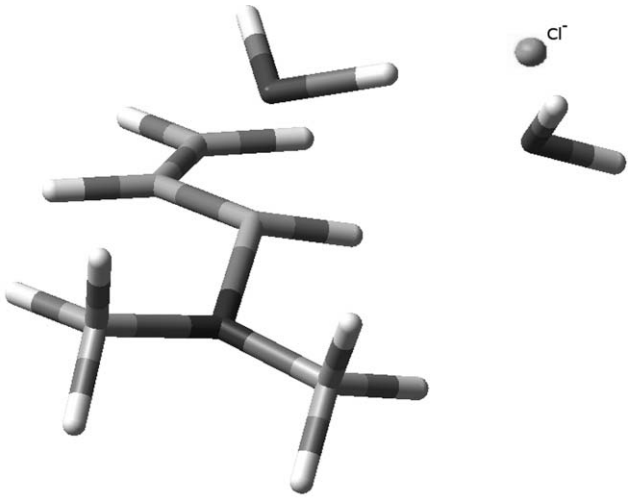

Fig. 7 TS3 geometry.

A final low energy minimum, corresponding to the iminium ion product after elimination of water from the aminol species, was located *ca.* 40 kJ mol^{-1} above the reactants. This product contains the expected N=C double bond, as evident by the planar disposition of groups about the new bond forming a sp^2 hybridised carbon centre, and a N=C length of 1.31 Å (Fig. 8). The chloride ion is now located above the N=C carbon, solvated by two explicit water molecules. Table 1 contains inter-atomic distances of N–C and C–O in the model reaction profile, as expected the general trend is toward formation of an N–C double bond and dissociation of C–O to give the iminium ion product.

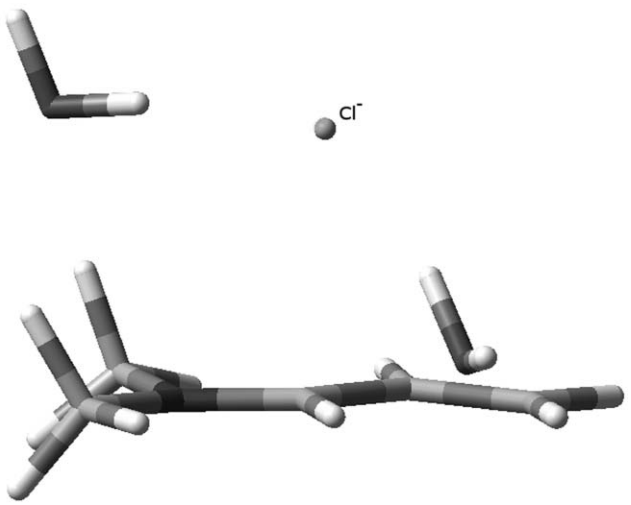

Fig. 8 Iminium ion product.

Table 1 Bond lengths over reaction profile

	Reactants	TS1	Intermediate	TS2	Aminol	TS3	Iminium product
N–C	3.637	4.437	2.771	2.272	1.558	1.390	1.305
C–O	1.233	1.229	1.232	1.257	1.377	1.617	3.961

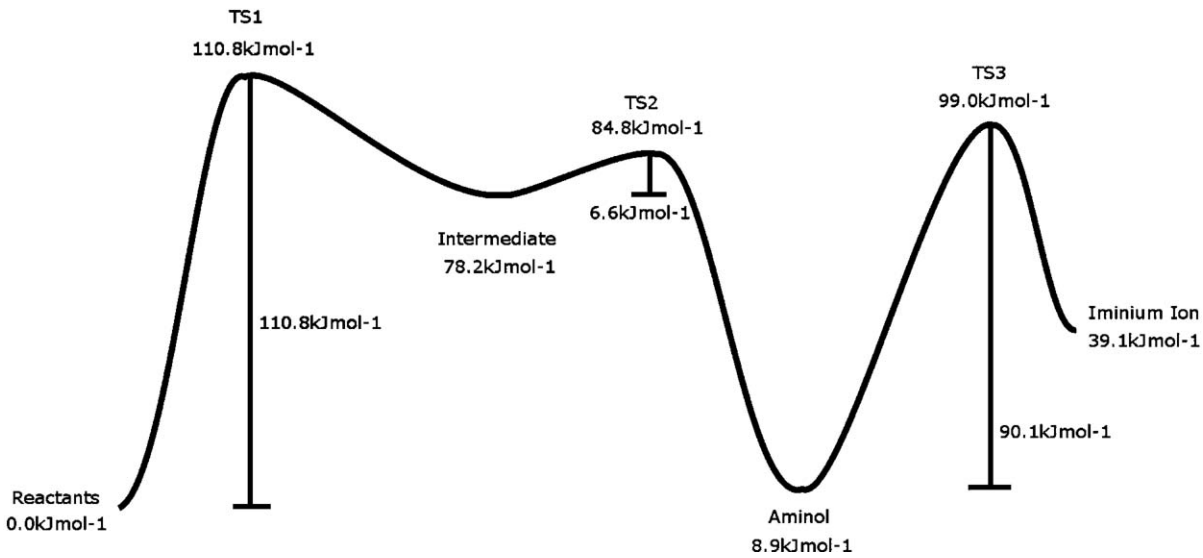

Scheme 2 Reaction profile of the reaction between dimethylamine hydrochloride and acrolein.

Therefore, our B3LYP/6-31+G(d,p)/Onsager calculations indicate a three-step, rather than a two-step mechanism for formation of an iminium ion from dimethylamine hydrochloride and acrolein, albeit with one energetically unimportant step, as shown in Scheme 2. There is therefore considerable scope for electronic and/or steric effects, through modification of the amine, to alter the kinetics of iminium ion formation.

Before moving on to studying these effects, we checked the stability of our results with respect to theoretical method, with results reported in Table 2. Expanding the basis set to 6-311++G(2d,p) reduces the energy of each stationary point relative to the reactant complex, the largest change being *ca.* 7 kJ mol^{-1} in TS1, with rather smaller changes elsewhere. Using the mPW1PW91 functional, reported to give improved barriers over B3LYP for model organic reactions,[32] has only a small effect on TS1, intermediate, and TS2 relative energies, but considerably reduces the energy of the aminol and TS3 structures, to the extent that the aminol intermediate is now lower in energy than the reactants. The difference in geometry between B3LYP and mPW1PW91 was essentially negligible.

We also checked the use of the polarisable continuum model (PCM) of solvation. We were unable to recalculate all stationary points shown in Scheme 2 using this method due to problems in calculating analytical second derivatives with PCM in Gaussian03. Instead, Table 2 and Fig. 9 contain single point B3LYP/6-31+G(d,p)/PCM energies at geometries from equivalent Onsager calculations. Barriers at TS1 and TS3 were consistently *ca.* 25 kJ mol^{-1} higher, perhaps due to the lack of geometrical relaxation at this level. Overall though, PCM solvation did not

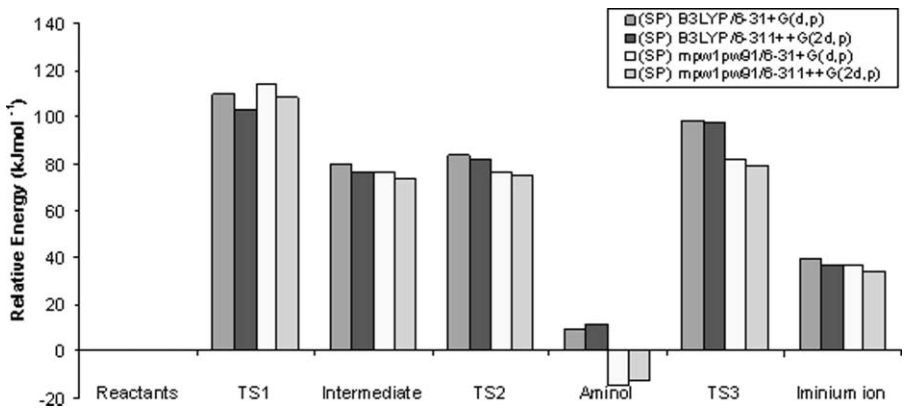

Fig. 9 Reaction profile at differing theory levels in PCM solvent.

Table 2 Energies of stationary points relative to reactant complex (kJ mol^{-1})

	TS1	Intermediate	TS2	Aminol	TS3	Iminium product
B3LYP/6-31+G(d)	109.7	80.1	83.8	9.7	98.7	39.4
B3LYP/6-311++G(2d,p)	102.9	76.9	82.2	11.6	97.9	36.8
mPW1PW91/6-31+G(d,p)	114.5	76.7	76.9	−14.7	81.7	37.0
B3LYP/6-31+G(d)+PCM	149.9	115.0	114.5	12.6	118.7	34.1

alter the calculated mechanism. Thus, both increasing the size of the basis set and using alternative DFT and solvation methods did not alter the fundamentals of our calculated mechanism.

The model dimethylamine system discussed above was used as a template for a number of cyclic and acyclic secondary amines (Fig. 10), with searches for stationary points starting from those found for dimethylamine. By overlaying a previously optimised amine over the dimethylamine of the model system an approximation for the stationary point was created. The majority of stationary points were found by standard optimisation techniques, but some more troublesome transition states were eluded with the QST3 method.

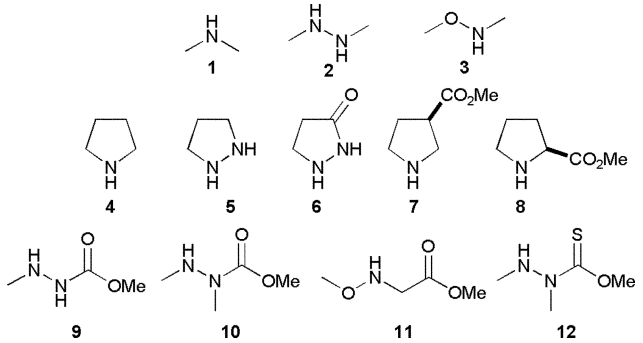

Fig. 10 Structures and numbering of secondary amines **1–12**.

The addition of a heteroatom (N or O) α- to the reactive nitrogen centre substantially decreases the barrier associated with TS1 (Fig. 11). The largest decrease (>25 kJ mol^{-1}) in barrier height was seen in **3**, reflecting the greater electronegativity of O over N, with a similar change in the energy at the intermediate geometry. The α-heteroatom did not significantly affect the geometry of the reactants, intermediate, or TS1, which suggests that the barrier reduction is largely electronic in nature. TS3 also lowers notably: in this case, energy differences appear to be due to the extra flexibility of the amine, as rotation around the N–X (X = N or O) bond allows further interactions with water and chloride. The presence of αN–H in **2** allows the formation of hydrogen bonding to O and Cl^-, which could also explain the relative stability of the iminium ion product of **2**.

The incorporation of the reactive secondary amine into the five-membered ring in pyrrolidine (**4**) increases TS1 to give the largest barrier found (118 kJ mol^{-1}). This amine also yields higher-energy of both remaining transition states, relative to **1** (Fig. 12). Substitution with α-nitrogen (**5**) gives a relative energy of TS1 below that of **1**, reinforcing the barrier-lowering effect of an α-heteroatom. Formation of hydrogen bonding between the α-N–H and acrolein is apparent in TS1, which may contribute to lowering the barrier by 19 kJ mol^{-1} *cf.* **4**. A decrease in relative energy *cf.* **4** is observed in the remaining two transition states and intermediate geometry, with corresponding increases in the relative energy of both aminol and iminium ion minima.

The effect of an endocyclic carbonyl group in the β-position of the five-membered ring can be seen in the data for the lactam **6**. This gives the lowest barrier to TS1 of all the data reported here, suggesting that this should form a useful catalyst. However, **6** also has the largest relative barriers associated with TS2 and TS3, such that TS3 lies only 1 kJ mol^{-1} below that of TS1. The hydrogen bonding network present in TS1 (Fig. 13) strongly

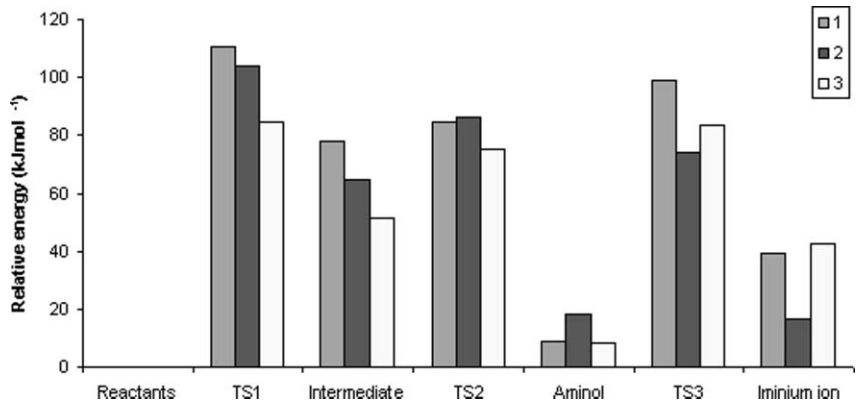

Fig. 11 Reaction profile for acyclic secondary amines **1–3**.

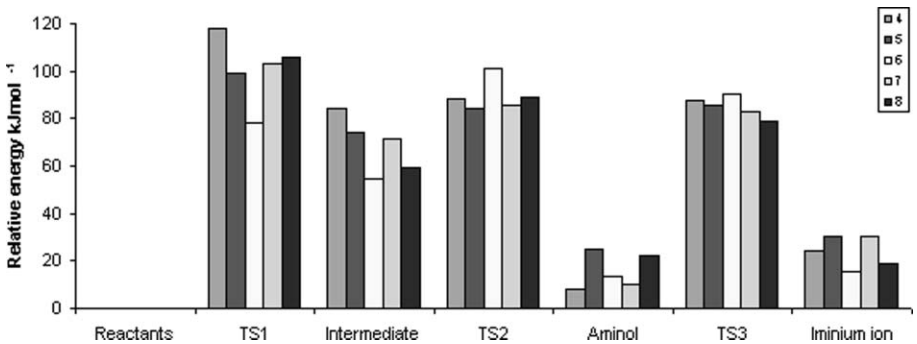

Fig. 12 Reaction profiles for cyclic secondary amines **4–8**.

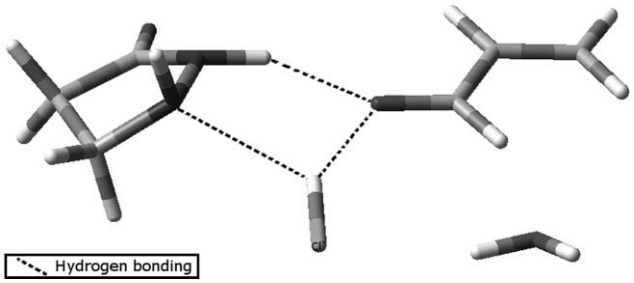

Fig. 13 Geometry of TS1 of **6**.

involves the α-N–H group, and causes the geometry to alter significantly compared with other molecules studied. Molecule **7**, which contains a carbonyl group but not the α-heteroatom, leads to a rather larger barrier associated with TS1, 15 kJ mol^{-1} larger than in **6**. The position of the carbonyl group (γ in **7**, β in **8**) appears to have little effect on the reaction profile, despite its closer proximity to the reactive centre in the latter.

The low TS1 barrier for the acyclic carbamates **9** and **10** (Fig. 14) supports the result for **6** that this functionality has a large effect on the reaction profile. In these acyclic cases, however, the relative energies of TS2 and TS3 are also significantly lower than found for other classes of amine. Substitution of hydrogen for methyl (*i.e.* **9** *cf.* **10**) has little effect on barriers, but the importance of the position of the α-heteroatom is highlighted by the data for **11**, whose TS1 is relatively high in energy compared to **9** and **10**, though this positioning has less of an effect on TS3. Interestingly, the lowest TS1 barrier found was that for the thiocarbamate **12**, which also shows subsequent barriers similar to the acyclic carbamates, and should therefore be at least as reactive as the carbamate. All carbamates considered stabilise the intermediate considerably, and increase the barrier at TS2 to the range between 20–40 kJ mol^{-1}. These carbamates (or thiocarbamates) form extensive hydrogen bonding networks through the carbonyl group (see Fig. 15), unlike **7** and **8** which are limited by the ring structure.

To explore more deeply the role of hydrogen bonding and other intermolecular interactions, and to follow the position of the reaction profile where bonds are formed and broken, we carried out AIM analysis of all stationary points, beginning with the model dimethylamine system. Visual inspection can identify the interactions within a certain structure, while the value of the electron density at the BCPs located allows interaction strengths to

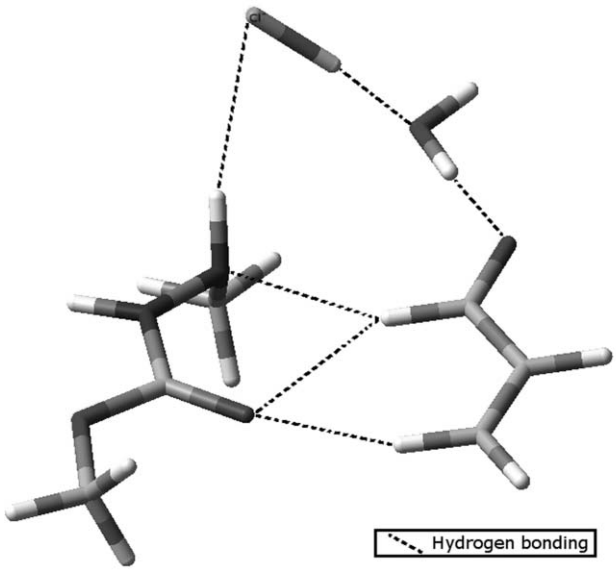

Fig. 15 Intermediate geometry of **10** showing hydrogen bonding network, including C–H · · · O interactions between β-carbonyl and acrolein.

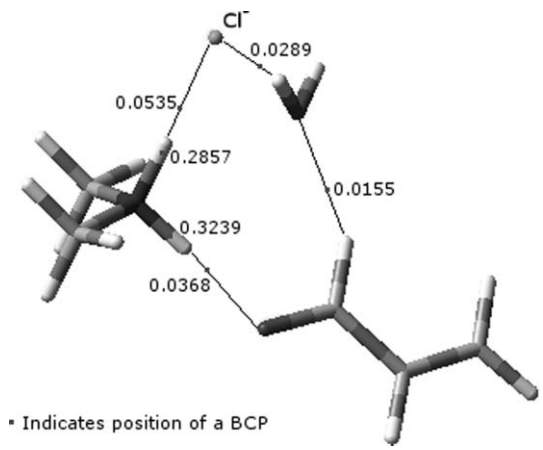

Fig. 16 Molecular graph of reactant of **1**, with ρ_{BCP} of significant intermolecular interactions indicated next to each BCP.

be quantified. The intermolecular interactions within the reactant ensemble are shown in Fig. 16. By some distance, the strongest interactions are those involving the protonated amine N–H, which forms H-bonds to the carbonyl and chloride. Remaining weaker

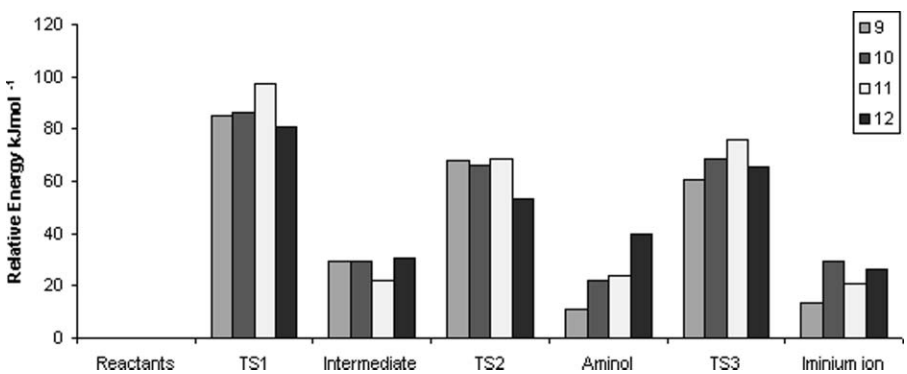

Fig. 14 Reaction profiles for carbamate derivatives **9–12**.

interactions involve the water molecule, which forms one O–H $\cdots$ Cl and two C–H $\cdots$ O H-bonds to acrolein and amine. The electron density at the BCP of the N–H coordinated to the chloride is lower than that of the N–H $\cdots$ O, indicating weakening of this bond due to the stronger H-bonding, and perhaps suggesting that the amine proton is more labile to the chloride.

At TS1, the proton has essentially been lost from N–H, with only a very weak interaction remaining: instead, a covalent H–Cl bond ($\rho = 0.230$ au) is present, along with a Cl–H $\cdots$ O H-bond to acrolein (Fig. 17). Stronger interaction of the transferred proton with the carbonyl oxygen than the nitrogen suggests a 'late' transition state. Orientation of the reactants appears to be moderated by H-bonding, with weak but symmetric contacts between carbonyl and methyl protons. The water molecule plays a passive role interacting with the chloride and α-proton of the acrolein similar to that of the reactants.

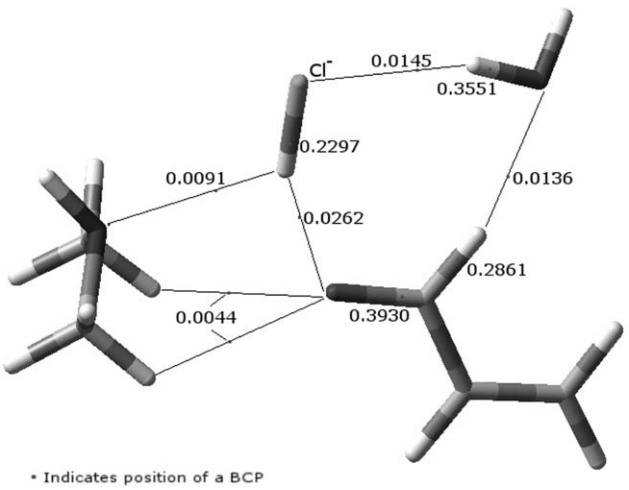

Fig. 17 Molecular graph of TS1 of **1**.

The intermediate geometry is the first in which an interaction between nitrogen and carbon is observed in the dimethylamine system (Fig. 18). To form this bond, acrolein must rotate relative to dimethylamine, and hence a number of interactions have been lost: the weak C–H $\cdots$ O interactions are replaced by stronger

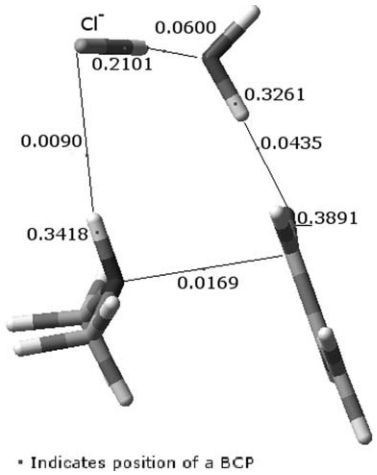

Fig. 18 Molecular graph of intermediate of **1**.

bonds involving the water molecule. Also the covalent H–Cl bond has greater interaction with water than in TS1.

TS2 is associated with a proton shuttle mechanism through H_2O, and hence there is no change in number and type of BCPs present from the intermediate (Fig. 19). However, AIM analysis shows the progress of proton transfer, with almost equal ρ at the Cl–H and H–O BCPs, such that the water might be better described as a hydronium ion here, along with weakened C–O and enhanced O $\cdots$ H interactions at the carbonyl. The incipient N–C bond is stronger here than in the intermediate, as is the N–H $\cdots$ Cl H-bond, since Cl is now more like a chloride ion here.

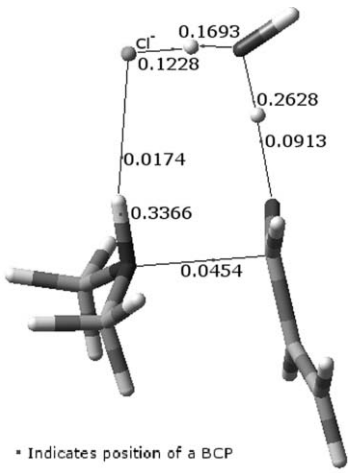

Fig. 19 Molecular graph of TS2 of **1**.

The aminol stationary point affords the first 'true' N–C bond (0.221 *cf.* 0.250 au in the N–C bond of dimethylamine), with ρ at the BCP almost five times that found at TS2, along with a protonated O–H at the former carbonyl and a weaker, longer C–O bond (Fig. 20). The chloride ion forms a strong H-bond to

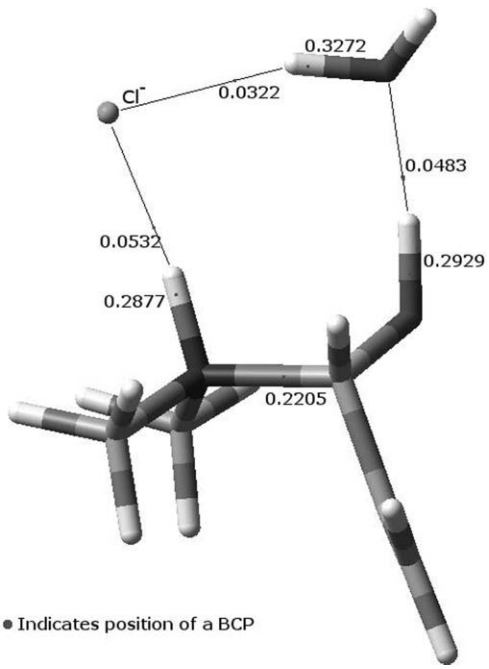

Fig. 20 Molecular graph of aminol of **1**.

the remaining amine proton, with similar electron density to that seen in the reactant. A strong O–H $\cdots$ O interaction is also seen between water and the now protonated carbonyl.

Formation of the final iminium ion product involves dehydration *via* transfer of the amine proton to the 'carbonyl' oxygen, which is accompanied by contraction of the N–C bond (Fig. 21). As in TS1, the chloride ion plays a key role in facilitating proton transfer, with almost equal sharing of electron density between H–Cl and O–H interactions at this TS. The strength of the N–C bond is again increased here compared to the aminol species, while the breaking C–O bond is considerably weaker. The water molecule interacts weakly with hydrogens from the dienophile and more strongly with the chloride.

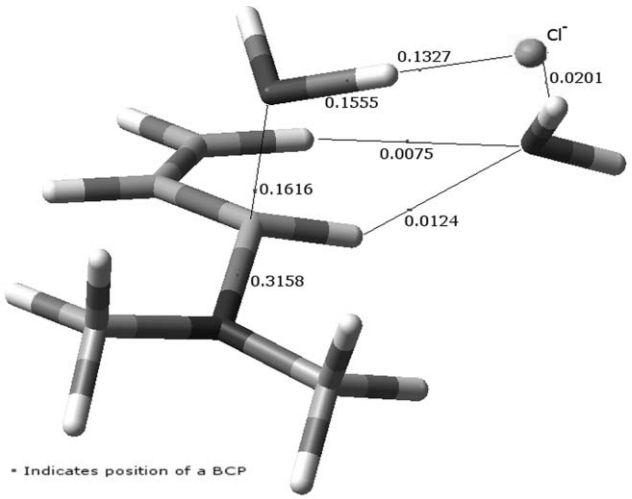

Fig. 21 Molecular graph of TS3 of **1**.

The final product of the profile is the iminium ion with $2H_2O + Cl^-$, which, as expected, has the largest ρ for the N–C bond observed thus far (Fig. 22). The positioning of the two water molecules allows each to have three H-bonding interactions of comparable strength. One water molecule interacts with the chloride and protons of the methyl groups, while the second

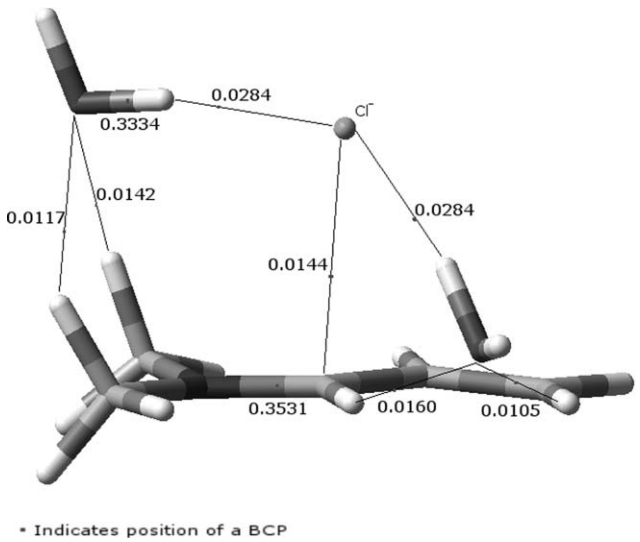

Fig. 22 Molecular graph of iminium ion of **1**.

accepts density from the protons of the alkene as well as donating to the chloride. The chloride centres above the carbon of the newly formed N=C bond, interacting directly with this atom. The essentially planar iminium ion also gives rise to weak H $\cdots$ H interaction between methyl and acrolein protons, a pattern similar to that recently studied by Matta *et al.*[33]

AIM analysis can also be used to shed light on possible reasons for the changes in relative energies with amine structures noted in Fig. 11–14. For instance, the low TS1 found for acyclic (thio)carbamates indicates that this functional group has direct bearing on the reaction profile: the relative energies of intermediate, TS2 and TS3 geometries are significantly lower than that of other classes of amine studied. These molecules form extensive hydrogen bonded networks, whose formation/disruption can play a role in the energetics of the reaction (Fig. 23). Such interactions cannot occur in cyclic molecules such as **7** and **8** due to the structural constraints of the ring.

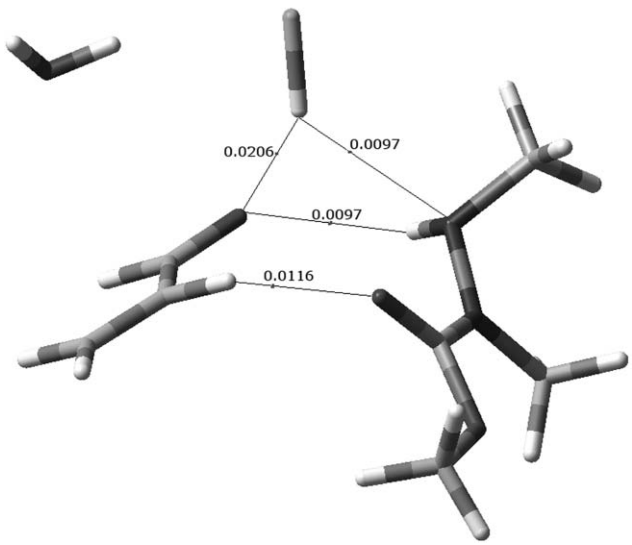

Fig. 23 Molecular graph of TS1 of **10**.

The presence of the C=O of carbamate has the effect of controlling the position of the acrolein, with interactions between protons in the early stages and carbon once the N–C bond has begun to form. The substitution of hydrogen for methyl (*cf.* **9** and **10**) has little effect on the reaction profile or the topology of the electron density. The importance of the position of the α-heteroatom is highlighted using **11**, in which TS1 has a relatively high barrier compared to the rest of the amines examined. However, once again the position of the reactants and the molecular graph is barely changed from that shown in Fig. 23.

The lowest TS1 of all molecules is found for compound **6**: the molecular graph (Fig. 24) of this shows the proton of the α-nitrogen forming an interaction (0.0209 au) with the acrolein oxygen. The formation of this interaction is at the expense of losing a slightly stronger (0.0277 au) interaction between α-nitrogen and water in the reactant complex. Thus, there appears to be a subtle interplay of formation and loss of hydrogen bonding contacts over the reaction profile, which along with the electronic variation at the reactive amine determines the overall barriers.

One consideration for non-symmetrical amines is the relative energy of *E* and *Z* configurations of the product iminium ion,

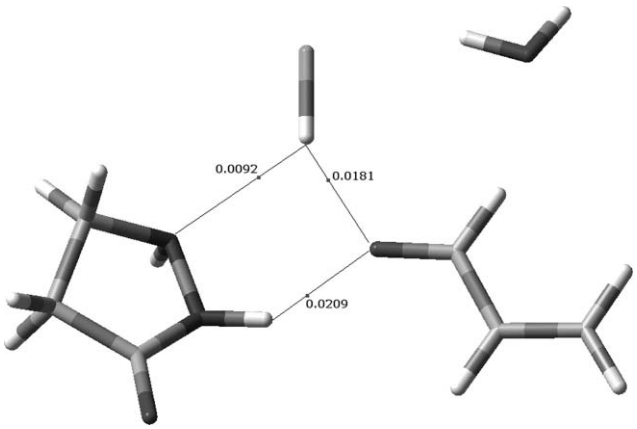

Fig. 24 Molecular graph of TS1 of **6**.

which may affect subsequent reactions *e.g.* by steric hindrance. The relative energies of *E* and *Z* orientations of four representative iminium ions formed from amines **2**, **3**, **5**, and **9** (Fig. 25) show, in each case, a small preference for the *Z* configuration. Conversion between isomers involves disruption of the π-system, and is therefore associated with a large barrier (*e.g.* 231.6 kJ mol^{-1} for **2**).

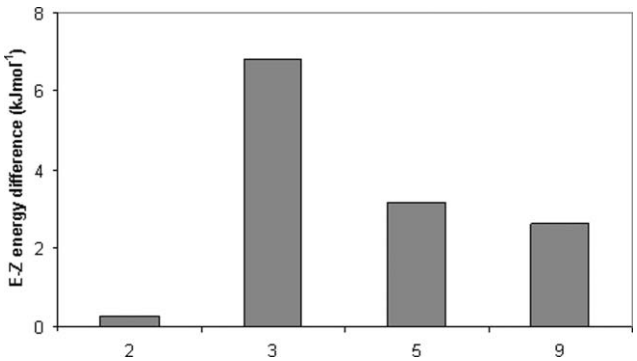

Fig. 25 Relative energy of *E*/*Z* configurations of four iminium ions.

This analysis raises the question of where in the reaction profile the issue of orientation of iminium ion and N-substituent first arises, *i.e.* where in the reaction profile does acrolein rotate to present the δ$^+$ carbonyl to the incoming nitrogen nucleophile. Our analysis (*e.g.* Fig. 13) shows that this occurs between the intermediate and aminol species, *i.e.* at TS2. We therefore searched for alternative geometries of TS2 for amines **2**, **3**, **5**, and **9**, in which the orientation of amine and acrolein is reversed from those shown and discussed above. In three of the four cases, we were unable to find a transition state corresponding to this altered pathway, so the above results appear to be the only feasible pathway to iminium formation. In these cases, the direction of rotation of acrolein is such that it leads to the energetically favoured *Z*-product, *i.e.* both kinetics and thermodynamics favour the formation of one product over another. For amine **5**, two geometries of TS2 were located, but these differ by 7 kJ mol^{-1}, an essentially negligible difference when compared to the barriers associated with TS1 and TS3.

Reaction profiles and AIM analysis indicate that the key factor in formation of an iminium ion is the transfer of a proton of the original protonated amine to the carbonyl of acrolein. Therefore, we investigated whether the basicity of the parent amine shows any relation to calculated barriers. Proton affinities (PA) of selected amines were evaluated at the same B3LYP/6-31+G(d,p) level, and are plotted in Fig. 26 alongside TS1 barriers. It is clear that there is some relation between the two values, which holds particularly well for the simple amines **1**–**3**. It appears that the relatively high barrier at TS1 found for pyrrolidine (**4**) is related to the high basicity of the parent amine, which would act to inhibit proton transfer, though the barrier for **6** is higher than might be expected on the basis of PA alone, perhaps due to the H-bond network noted above.

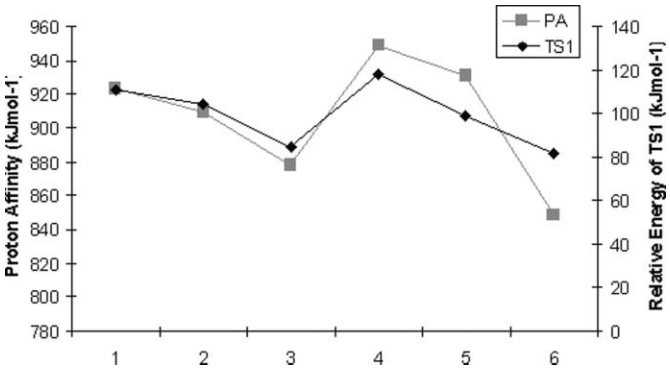

Fig. 26 B3LYP/6-31+G(d,p) proton affinities and TS1 barriers (kJ mol^{-1}).

It is revealing to compare the energetics of reaction profiles calculated in this work with overall catalytic yields for the cycle shown in Scheme 1. Table 3 contains four such yields for four amines, where experimental yields correspond to a common reaction time of 72 hours and standardised reaction conditions, along with calculated barriers at TS1. These data indicate that the low TS1 barrier for amine **3** does indeed correspond to greater catalytic efficiency, whereas simple amines **1** and **4** have high TS1 barriers and are poor catalysts. Such comparison for the hydrazine derivative **3** is complicated by the fact that experimentally this is present as the di-hydrochloride salt (MeNH–NHMe·2HCl), whereas in our calculations only the mono-hydrochloride salt was considered, for consistency with other amines. Also, amines **1**, **2**, and **4** show a clear preference for *exo* over *endo* Diels–Alder products, whereas **3** shows the opposite stereochemistry, which may be indicative of an alternative pathway for this case. Overall, it seems clear that a lower TS1 barrier leads to greater catalytic efficiency, though more data is required before quantitative predictions can be made.

The comparisons shown in Table 3 prompted us to explore, at the same theoretical level, the subsequent Diels–Alder reaction of iminium ions based on acrolein and amines **1**–**4**. In the

Table 3 Comparison of TS1 barriers and experimental yields

	Δ*E* TS1/ kJ mol^{-1}	Yield (%) (72 hours)[a]	*Endo* : *exo* ratio[b]
Pyrrolidine (**4**)	118.03	27	32 : 68
Dimethylamine (**1**)	110.80	29	35 : 65
Dimethylhydrazine (**2**)	104.23	48	68 : 32
Dimethylhydroxylamine (**3**)	84.80	80	34 : 66

[a] Standardised reaction conditions of cinnamaldehyde (1 eq.) and cyclopentadiene (3 eq.) in a 19 : 1 methanol–water mixture @ 25 °C for 72 h. [b] Determined by ^{1}H NMR of crude reaction mixture.

Table 4 Barriers to Diels–Alder cycloaddition reaction (kJ mol^{-1})

		No solvent	Onsager	PCM
Acrolein	*Exo*	81.5	80.3	68.5
	Endo	84.3	83.2	67.7
Iminium **1**	*Exo*	21.6	25.7	31.2
	Endo	21.1	25.5	30.7
Iminium **2**	*Exo*	50.4	52.5	45.2
	Endo	49.9	52.2	43.8
Iminium **3**	*Exo*	14.2	16.3	13.4
	Endo	13.1	15.0	12.3
Iminium **4**	*Exo*	29.9	31.5	33.6
	Endo	29.4	31.0	33.1

absence of any solvent, acrolein itself undergoes cycloaddition with cyclopentadiene with a barrier of 81.5 kJ mol^{-1} for the *exo* pathway and 84.3 kJ mol^{-1} for *endo* (see Table 4). These barriers are substantially reduced for the iminium ion formed from acrolein plus amine **1**: barriers of between 21 and 25 kJ mol^{-1} are found, depending on solvent model and *endo*/*exo* pathway. This is consistent with the general principles of organocatalysis of Diels–Alder cycloaddition, in which the substrate double bond is activated, and also with literature expectations of iminium ion catalysis, where formation of an iminium ion is believed to be the rate determining step.

Table 4 also compares barriers to reaction for amines **1–4**, which shows that amine structure has some influence on this stage of the catalytic cycle. For instance, the iminium ion based on dimethylhydrazine (**2**) and acrolein has a rather larger barrier than all other amines, whereas that from **3** plus acrolein has a very low barrier for Diels–Alder reaction. However, in all cases barriers are substantially lower than for acrolein itself, suggesting that they all activate the dienophile. Comparison of Table 4 with Fig. 9–12 shows that barriers to formation of iminium ions are greater than, or at best similar to, that for direct Diels–Alder reaction of unmodified acrolein, such that over the entire cycle shown in Scheme 1 no catalysis occurs. This apparent discrepancy might be explained by the fact that experimental data is obtained using cinnamaldehyde (3-phenylprop-2-enal) rather than acrolein. This is significantly less reactive in the Diels–Alder step than acrolein, with a calculated barrier of 112 kJ mol^{-1}, *i.e.* 30 kJ mol^{-1} more than acrolein in the same conditions. We anticipate that phenyl substitution will not have such a large effect on barriers to iminium ion formation: calculations are underway to confirm this. Also, throughout Table 4, we find no evidence for significant differences in energy barriers between *endo* and *exo* pathways: further work is underway to explore the origin of the observed stereochemistry.

Conclusions

Density functional calculations have been performed for the formation of an iminium ion from a variety of protonated amines plus acrolein in aqueous methanol. From these calculations, we find that substitution of the amine gives clear changes in activation barriers on the reaction profile. Inclusion of a heteroatom α- to the reactive secondary amine centre reduces the energetic barrier in all cases, while addition of an electron-withdrawing carbonyl or thiocarbonyl to this heteroatom further reduces barriers. This is found to be most effective in acyclic amines, apparently due to the extra flexibility of these over cyclic species.

Deprotonation of the amine is found to be the rate-determining step in the formation of the iminium ion, and hence possibly of the overall catalytic Diels–Alder reaction shown in Scheme 1. Atoms in Molecules (AIM) analysis confirms that loss of a proton from the protonated amine is the key change in this rate-determining step. Comparison of the first proton abstraction (TS1) and rates of conversion over 72 hours was made, which appears to show some relation of theoretical and experimental values. Moreover, we find some correlation between the calculated proton affinity of the free amines and the barrier of the rate-determining step, opening up the possibility of simple prediction of reactivity from PA.

Acknowledgements

This work was funded under EPSRC grant ref GR/S69337/01. All calculations were carried out on Cardiff University's Helix Computation and Visualisation Facility.

References

1 J. Seayad and B. List, *Org. Biomol. Chem.*, 2005, **3**, 719–724.
2 P. I. Dalko and L. Moisan, *Angew. Chem., Int. Ed.*, 2001, **40**, 3726–3748.
3 P. I. Dalko and L. Moisan, *Angew. Chem., Int. Ed.*, 2004, **43**, 5138–5175.
4 K. A. Ahrendt, C. J. Borths and D. W. C. MacMillan, *J. Am. Chem. Soc.*, 2000, **122**, 4243–4244.
5 J. F. Austin and D. W. C. MacMillan, *J. Am. Chem. Soc.*, 2002, **124**, 1172–1173.
6 M. Harmata, S. K. Ghosh, X. C. Hong, S. Wacharasindhu and P. Kirchhoefer, *J. Am. Chem. Soc.*, 2003, **125**, 2058–2059.
7 W. Notz and B. List, *J. Am. Chem. Soc.*, 2000, **122**, 7386–7387.
8 N. A. Paras and D. W. C. MacMillan, *J. Am. Chem. Soc.*, 2001, **123**, 4370–4371.
9 N. A. Paras and D. W. C. MacMillan, *J. Am. Chem. Soc.*, 2002, **124**, 7894–7895.
10 N. Yoshikawa, T. Suzuki and M. Shibasaki, *J. Org. Chem.*, 2002, **67**, 2556–2565.
11 W. S. Jen, J. J. M. Wiener and D. W. C. MacMillan, *J. Am. Chem. Soc.*, 2000, **122**, 9874–9875.
12 J. L. Cavill, J. U. Peters and N. C. O. Tomkinson, *Chem. Commun.*, 2003, 728–729.
13 W. P. Jencks, *Catalysis in Chemistry and Enzymology*, McGraw Hill Text, New York, 1969.
14 R. Gordillo, J. Carter and K. N. Houk, *Adv. Synth. Catal.*, 2004, **346**, 1175–1185.
15 C. Allemann, R. Gordillo, F. R. Clemente, P. H. Y. Cheong and K. N. Houk, *Acc. Chem. Res.*, 2004, **37**, 558–569.
16 K. N. Rankin, J. W. Gauld and R. J. Boyd, *J. Phys. Chem. A*, 2002, **106**, 5155–5159.
17 Gaussian 03, Revision B.05, M. J. Frisch, G. W. Trucks, H. B. Schlegel, G. E. Scuseria, M. A. Robb, J. R. Cheeseman, J. A. Montgomery, Jr., T. Vreven, K. N. Kudin, J. C. Burant, J. M. Millam, S. S. Iyengar, J. Tomasi, V. Barone, B. Mennucci, M. Cossi, G. Scalmani, N. Rega, G. A. Petersson, H. Nakatsuji, M. Hada, M. Ehara, K. Toyota, R. Fukuda, J. Hasegawa, M. Ishida, T. Nakajima, Y. Honda, O. Kitao, H. Nakai, M. Klene, X. Li, J. E. Knox, H. P. Hratchian, J. B. Cross, C. Adamo, J. Jaramillo, R. Gomperts, R. E. Stratmann, O. Yazyev, A. J. Austin, R. Cammi, C. Pomelli, J. W. Ochterski, P. Y. Ayala, K. Morokuma, G. A. Voth, P. Salvador, J. J. Dannenberg, V. G. Zakrzewski, S. Dapprich, A. D. Daniels, M. C. Strain, O. Farkas, D. K. Malick, A. D. Rabuck, K. Raghavachari, J. B. Foresman, J. V. Ortiz, Q. Cui, A. G. Baboul, S. Clifford, J. Cioslowski, B. B. Stefanov, G. Liu, A. Liashenko, P. Piskorz, I. Komaromi, R. L. Martin, D. J. Fox, T. Keith, M. A. Al-Laham, C. Y. Peng, A. Nanayakkara, M. Challacombe, P. M. W. Gill, B. Johnson, W. Chen, M. W. Wong, C. Gonzalez and J. A. Pople, Gaussian, Inc., Pittsburgh, PA, 2003.
18 A. D. Becke, *Phys. Rev. A*, 1988, **38**, 3098–3100.

19 C. T. Lee, W. T. Yang and R. G. Parr, *Phys. Rev. B*, 1988, **37**, 785–789.
20 M. J. Frisch, J. A. Pople and J. S. Binkley, *J. Chem. Phys.*, 1984, **80**, 3265–3269.
21 L. Onsager, *J. Am. Chem. Soc.*, 1936, **158**, 1486.
22 C. Adamo and V. Barone, *J. Chem. Phys.*, 1998, **108**, 664–675.
23 J. Tomasi, B. Mennucci and E. Cances, *J. Mol. Struct. (THEOCHEM)*, 1999, **464**, 211–226.
24 C. Peng and H. B. Schlegel, *Isr. J. Chem.*, 1994, **33**, 449.
25 C. Peng, P. Y. Ayala, H. B. Schlegel and M. J. Frisch, *J. Comput. Chem.*, 1996, **17**, 49.
26 F. Biegler-König, J. Schönbohm and D. Bayles, *J. Comput. Chem.*, 2001, **22**, 545–559.
27 R. F. W. Bader, *Atoms in Molecules—A Quantum Theory*, Oxford University Press, Oxford, 1990.
28 P. L. A. Popelier, *Atoms in Molecules: An Introduction*, Prentice Hall, Harlow, 2000.
29 S. T. Howard and O. Lamarche, *J. Phys. Org. Chem.*, 2003, **16**, 133–141.
30 R. F. W. Bader, T. S. Slee, D. Cremer and E. Kraka, *J. Am. Chem. Soc.*, 1983, **105**, 5061–5068.
31 D. Cremer and E. Kraka, *Angew. Chem., Int. Ed. Engl.*, 1984, **23**, 627–628.
32 B. J. Lynch and D. G. Truhlar, *J. Phys. Chem. A*, 2001, **105**, 2936–2941.
33 C. F. Matta, J. Hernandez-Trujillo, T. H. Tang and R. F. W. Bader, *Chem.–Eur. J.*, 2003, **9**, 1940–1951.